The 12th Swedish
Aerospace Technology Congress
FT2025 in Stockholm
October 14-15, 2025

Experimental Evaluation of Classical Washout Filter Configurations for Fighter Jet Motion Cueing

Yasmin Castro¹, Andrew Sarmento¹, Emilia Villani¹ and Wesley Oliveira¹

¹ Competence Center in Manufacturing (CCM), Aeronautics Institute of Technology (ITA), São José dos Campos, Brazil E-mail: yasmin.castro@ccm-ita.org.br, andrewgps@ccm-ita.org.br, emilia.villani@ccm-ita.org.br, wesleyo@ccm-ita.org.br

Abstract

This research presents an exploratory investigation on the performance of classical washout filter configurations in replicating the motion dynamics of a fighter aircraft on the SIVOR platform, which is a flight simulator with a 7 dof robotic arm. Using the ADMIRE model to simulate flight dynamics, two washout configurations (baseline and tuned) were evaluated under smooth and aggressive commands for the same set of maneuvers. The simulator's end-effector motion was compared to the aircraft's original dynamics using a vestibular system model, incorporating human perception thresholds to quantify perceptual mismatch. Root Mean Square Error (RMSE) and normalized cross-correlation were computed to assess cue fidelity across flight segments between the expected aircraft flight and the simulated flights. Additionally, CoppeliaSim is employed to simulate and visualize SIVOR's behavior during each test case to evaluate collision occurrences in advance. Although the tuned MCA demonstrated marginal improvement over the baseline, both algorithms failed to consistently represent the fighter motion accurately. Results revealed that fixed-parameter filters underperformed not only across different maneuver types, but also for variations within the same maneuver due to small changes in control inputs. These initial findings are in agreement with literature, which highlights the limitations of classical washout filters and emphasize the need for adaptive or model-predictive cueing strategies, especially for high-gain flight scenarios.

Keywords: Motion Cueing, Flight Simulation, Washout Filter, Fighter Aircraft

1 Introduction

Flight simulators play a crucial role in various aerospace applications, ranging from pilot training and certification to research and the development of advanced flight technologies. Among the different types of simulators, fullmotion platforms offer a unique advantage by providing realistic physical sensations that resemble those experienced in real flight [1]. However, achieving such realism is inherently constrained by the physical limitations of the simulator's motion envelope. To address this, motion cueing algorithms (MCAs) are employed to translate the full-scale aircraft dynamics into motions that can be reproduced within the simulator's restricted workspace, while still preserving perceptual fidelity for the pilot. The effectiveness of a motion cueing algorithm depends heavily on proper parameter tuning, as it directly impacts how motion cues are generated and perceived [2].

Various approaches of MCAs exist, ranging from simple offline parametrization to model-based predictive-control techniques [3][4]. Among them, the classical washout filter remains one of the most widely used, especially in transport aviation contexts, due to its simplicity, robustness, and relatively low computational cost [1][2]. It operates by

filtering high-frequency motion cues directly to the platform while gradually "washing out" low-frequency components to avoid exceeding the system's workspace limits [5]. However, its application in high-performance aircraft simulations remains relatively underexplored, particularly when attempting to replicate the more aggressive maneuvers and dynamic responses typical of fighter jets.

The SIVOR [1][6], in Figure 1, is a 7-degree-of-freedom (7-DoF) full-motion simulator designed primarily for executive aircraft. Its motion cueing system is currently tuned for an executive-class jet model, reflecting the flight characteristics of a small-size business jet. In the context of expanding SIVOR's capabilities to support a broader range of aircraft, this paper recovers the ADMIRE model [7], a nonlinear representation of a modern fighter jet, into the SIVOR simulation environment. The transition to a high-gain aircraft model poses significant challenges to the existing washout filter configuration, which may not adequately replicate the dynamic cues required for realistic simulation. Nevertheless, investigating its limitations when applied to these scenarios provides valuable insight into whether it can adequately convey such motions drawing requirements for an specific cueing technique.



Figure 1: SIVOR.

This paper presents an investigation into the performance of classical washout filter configurations when applied to the ADMIRE model within the SIVOR platform. The goal is to evaluate how effectively the existing motion cueing setup can convey the movement of a spry aircraft, identifying the limitations that arise in this context. The findings aim to provide insight into the requirements of MCA techniques for fighter aircraft simulation and support future efforts in SIVOR motion cueing for enhanced pilot perception and performance.

2 Methodology

This study is conducted by recording pilot-executed maneuvers using the ADMIRE aircraft model and analyzing the resulting perception mismatch—defined as the error in perceived motion according to a vestibular system model—after the aircraft dynamics are processed through the washout filter under different tuning configurations and the dynamic model of the motion platform.

The model-based method followed in this work is represented in Figure 2.

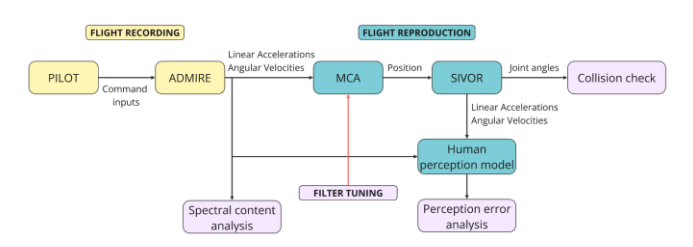


Figure 2: Simplified workflow of the study.

First, the set of maneuvers used in the experiment is defined, as described in Section 2.1. These maneuvers were then performed using the ADMIRE model, and the resulting aircraft motion data are recorded. Section 2.2 presents a frequency-domain analysis of these signals, which intends: (1) to assess whether the motion characteristics of the maneuvers fall within the capabilities of the KUKA KR 1000 TITAN robotic arm, and (2) to identify the dominant frequency components excited during the maneuvers based on their power spectra.

Section 2.3 details the vestibular system model used to estimate the pilot's motion perception based on both the aircraft's dynamics and the simulator's output. The classical washout filter configurations used in the study are described in Section 2.4. By applying the filter to the recorded aircraft motions, the resulting simulator output was compared to the original aircraft dynamics using the vestibular model to compute the perception mismatch.

Finally, Section 2.5 explains how this mismatch was quantified and interpreted. This includes considerations related to the simulator's workspace, collision avoidance constraints, and their impact on motion cueing fidelity and the accuracy of perceived motion.

2.1 Maneuvers

The maneuvers chosen for this experiment were inspired by the findings from [8], where coordinated turns were identified as the maneuvers most prone to perception mismatch even when using optimized MCA. The underlying study involved a subjective evaluation, developed in [9], in which expert drivers continuously rated the mismatch between the motion experienced in the simulator and the expected motion of a real vehicle. As result, coordinated turns yielded the highest mismatch ratings.

To explore the simulator's capability to reproduce circular motion, assumed to be the condition with the highest likelihood of mismatch, a volunteer military fighter pilot was asked to perform the four maneuvers shown in Figure 3.

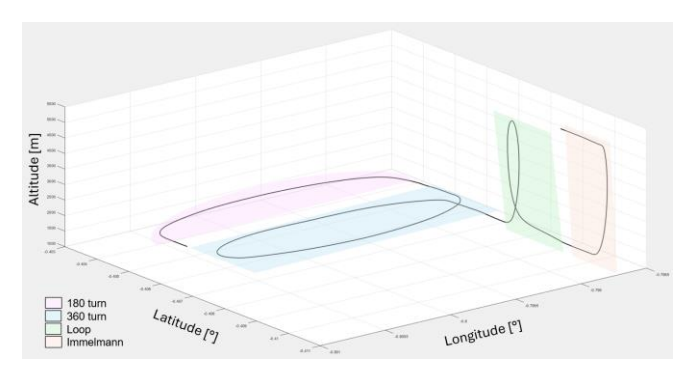


Figure 3: Flight Path

Figure 3 illustrates the flight path traced during the experiment, as recorded from the ADMIRE model. Each

segment of the trajectory is highlighted according to the maneuver performed. The sequence begins with a 180° turn (pink), followed by a 360° turn (blue), then a loop (green), and finally an Immelmann turn (orange)—a half-loop followed by a roll, resulting in a reversal of heading while gaining altitude.

To ensure clear segmentation of the data and facilitate subsequent analysis, approximately 10 seconds of level flight were maintained between each maneuver. These intervals serve not only as temporal markers for defining the start and end of each task in the signal recordings, but also provide insight into simulator behavior during transitions from equilibrium conditions.

Each maneuver was executed twice, across two flights: the first pass was performed in a smooth and controlled manner and without using afterburner, while the second focused solely on completing the task, allowing for more abrupt or aggressive control inputs. This dual execution strategy is designed to investigate how the simulator responds to different dynamic profiles, particularly on how it handles transitions to faster and more demanding motion cues.

2.2 Frequency analysis

Although robotic-arm-based simulators such as SIVOR offer a more versatile workspace compared to traditional Stewart platforms [10], the success of motion cueing remains constrained by the robot's ability to reproduce the motion demands imposed by the simulated aircraft.

To evaluate whether the KUKA KR 1000 TITAN can accommodate the dynamics of the ADMIRE model, a time-frequency analysis was conducted on the interest signals generated during the experimental maneuvers for both fights. Specifically, linear accelerations and angular velocities—used as inputs to the motion cueing algorithm—were all analyzed through their spectral content, as exemplified by Figures 4 and 5. In these figures, the dashed lines delimit the maneuvers (1) 180° turn, (2) 360° turn, (3) loop and (4) Immelmann turn.

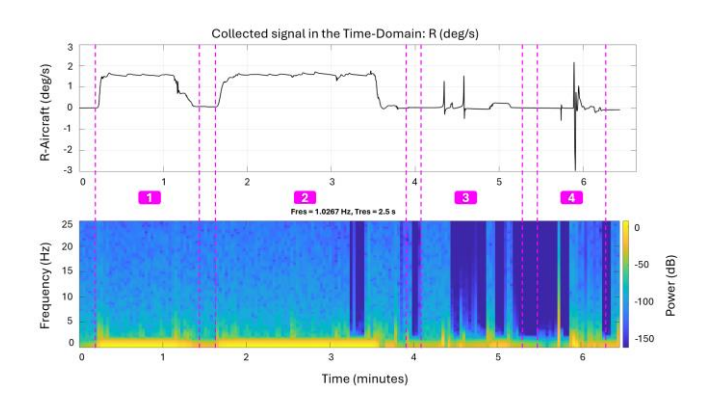


Figure 4: Yaw signal (R) recorded from the Smooth pass

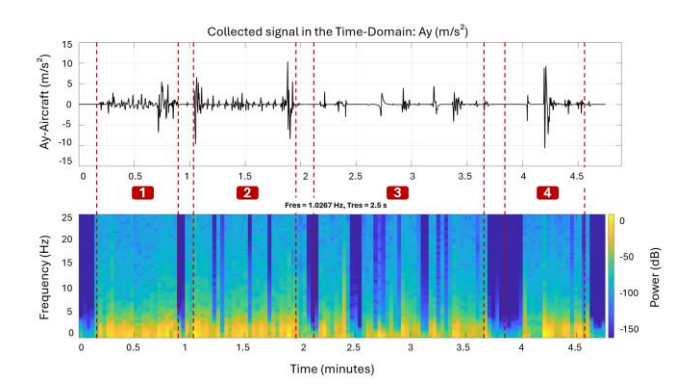


Figure 5: Y acceleration (Ay) signal recorded from Aggressive run

For each signal, the power spectrum is analyzed to identify the frequencies excited during the maneuvers, with the relevant components concentrated in the warmer region of the respective window. As expected, the aggressive run exhibited slightly higher magnitudes in the relevant frequency band compared to the smooth pass. However, even under aggressive inputs, no significant frequency components were observed beyond 6 Hz—which is suggested to be the resonance frequency of the robotic arm according to [11]. Based on this, the maneuvers are considered to lie within the robot's bandwidth.

2.3 Human Perception

A critical aspect of motion simulator design is to account for how motion is perceived by the human pilot. The goal is to replicate the sensation of being in a real vehicle as closely as possible, meaning that the motion experienced inside the simulator must be perceptually consistent with that of the actual aircraft. The closer the perceived motion is to reality, the more effective the MCA is at delivering representative cues.

To address the 'representativeness' of motion cues in a model-based analysis, this study adopts the classical vestibular system model to approximate human motion perception. This system, responsible for balance and spatial orientation, provides a biologically grounded way to assess how well simulated motion is interpreted by the human body [12]. While a complete perception model—encompassing vestibular, visual, and proprioceptive inputs—could offer greater fidelity, such models are highly task-dependent and often impractical to implement comprehensively for exploratory study, as noted by [2].

The vestibular system consists primarily of two components: the otolith organs, which detect linear acceleration, and the semicircular canals, which detect angular velocity. This work considers the vestibular system model of [13] as described in [12][14] to be suited for motion cueing algorithms, with Equation 1 representing the otolith model and Equation 2 the semicircular channel.

$$\frac{\hat{f}(s)}{f(s)} = \frac{4s + 0.4}{0.08s^2 + 5.016s + 1} \tag{1}$$

$$\frac{\widehat{\omega}(s)}{\omega(s)} = \frac{458.4s^2}{458.4s^2 + 85.73s + 1} \tag{2}$$

Where \hat{f} , f, $\hat{\omega}$ and ω stand for sensed specific force, specific force input, sensed angular velocity and angular velocity input respectively.

2.4 Motion Cueing Algorithm

In this study, the classical washout filter is employed to assess its capability in conveying fighter jet dynamics within the SIVOR platform. The filter, illustrated in Figure 6, is composed of separate high-pass and low-pass components applied to linear accelerations and angular velocities, with the objective of preserving perceptually important cues while managing simulator constraints.

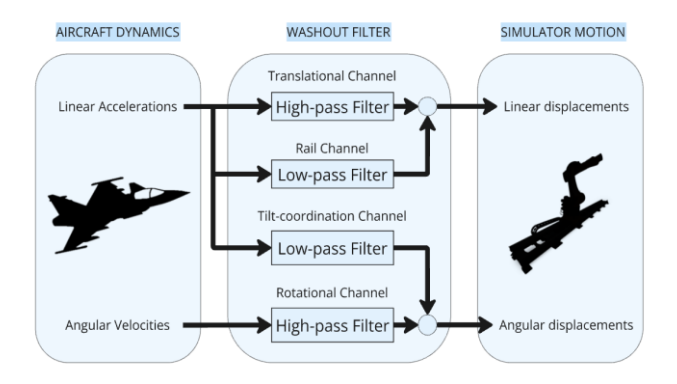


Figure 6: SIVOR Classical Washout Filter.

The current version of washout used in SIVOR, which here serves as baseline, follows the described in [15] for the translational, rotational and tilt coordination channels—Equations 3 to 5, respectively. While the additional rail channel is defined as in [15] as a second order low-pass filter that can also be represented by Equation 5.

$$G(s) = \frac{s^2}{s^2 + 2\zeta\omega_n s + \omega_n^2}$$
 (3)

$$G(s) = \frac{s}{s + \omega_{\rm n}} \tag{4}$$

$$G(s) = \frac{{\omega_{\rm n}}^2}{s^2 + 2\zeta\omega_{\rm n}s + {\omega_{\rm n}}^2}$$
 (5)

In the translational channel filter, the ζ is equal to 1 and ω_n to 2.5 rad/s for X and 4 rad/s for Y and Z. For the rotational channel, ω_n is 1 rad/s for all axes. The tilt coordination has ζ equal to 1, ω_n 5 rad/s for X and 8 rad/s for Y. Finally, in the rail channel ζ is equal to 0.7 and ω_n to 0.6283 rad/s.

This configuration is preserved, but its parameters are then adjusted in this paper so that the comparison between baseline and a possible tuned version is carried out.

The washout filter tuning is performed with the following considerations in mind:

- Maneuver dynamics, based on the recorded responses from ADMIRE during the selected experimental maneuvers (Section 2.1), to ensure that the filter responds appropriately to different intensity levels of motion.
- Robot capabilities, as evaluated through frequency-domain analysis (Section 2.2), ensuring that commanded motions do not exceed the effective frequency bandwidth of the KUKA KR 1000 TITAN. Additionally, the physical limitations of the platform are then addressed by looking for possible collisions between cockpit and robot.
- Perceptual relevance, using the vestibular system model described in Section 2.3 to evaluate whether the resulting cues fall within human perceptual thresholds used in the error analysis in 2.5.

2.5 Performance analysis

To assess the effectiveness of the MCAs, a comparison is conducted between the dynamic outputs of the pilot model within the aircraft model and the corresponding motions felt by the pilot within the simulator platform. Specifically, the linear accelerations and angular velocities generated by the ADMIRE simulation are compared to the same variables obtained at the robot end-effector after processing through the classical washout filter, as was presented in Figure 2. This comparison provides insight into how accurately the SIVOR platform conveys the intended motion cues.

Aircraft and simulator outputs are passed through the vestibular system model described in Section 2.3. This transformation simulates how the pilot perceives the motion through the human balance and spatial orientation system. Then, by comparing the vestibular outputs from both paths, the mismatch is computed taking into account the human perception thresholds. In this study, these values are set at 0.08 m/s² for linear acceleration and 3°/s for angular velocity [13]. Signal differences falling within these thresholds are considered imperceptible and, therefore, not contributors to perceived error. It is worth noting that although recent studies [16] suggest the rotational perception threshold can vary depending on the task (reporting values as high as 12°/s) the 3°/s threshold adopted here provides a conservative and suitable reference for our exploratory investigation avoiding the risk of allowing false cues to pass. This ensures the analysis remains grounded in human sensory resolution, aligning the evaluation metric with real-world perceptual fidelity.

In addition to visualizing the mismatch over time, two metrics are used to compare the quality of motion reproduction: root mean square error (RMSE) and normalized cross-correlation (R). The RMSE quantifies the average magnitude of deviation between the aircraft and simulator vestibular signals and is defined in Equation 6 [17] as:

$$E = \sqrt{\frac{1}{n} \sum_{i=1}^{n} |A_i - F_i|^2}$$
 (6)

where A_i is the actual signal (aircraft) perceived by the pilot (output at the vestibular model), F_i is the same reproduced signal in simulator, and n is the number of signal samples.

The normalized cross-correlation coefficient evaluates the shape and phase similarity between the signals, independent of their amplitude, and is computed in Equation 7 [18] as:

$$\hat{R}_{xy,coeff}(m) = \frac{1}{\sqrt{\hat{R}_{xx}(0)\hat{R}_{yy}(0)}} \hat{R}_{xy}(m)$$
(7)

In this study, it is base on the function "xcorr" from Matlab, and the values of interest are defined for zero lag (m = 0).

3 Results and Discussion

This section presents the results from the tuning process of the classical washout filter, comparing the newly configured version to the baseline and evaluating the suitability of both for representing the ADMIRE aircraft dynamics. The pilot's perceived motion, as computed from the vestibular model, serves as the reference for ideal cueing performance—illustrated in Figure 7 for the smooth-run maneuvers and Figure 8 for the aggressive inputs. In an ideal scenario, the pilot inside the simulator would experience motion cues indistinguishable from those felt during the actual aircraft flight.

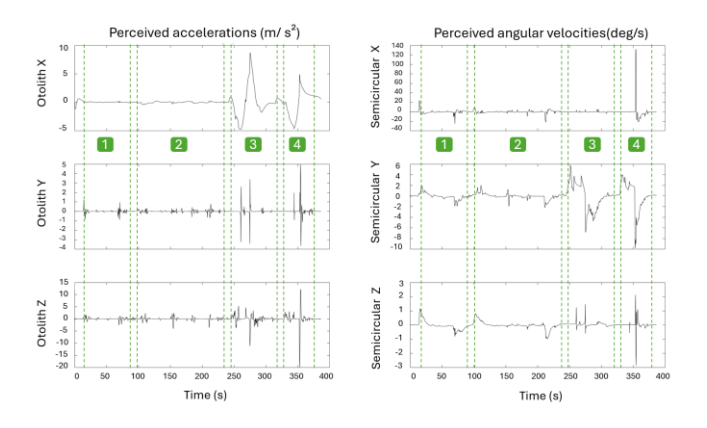


Figure 7: Perceived motion - Smooth

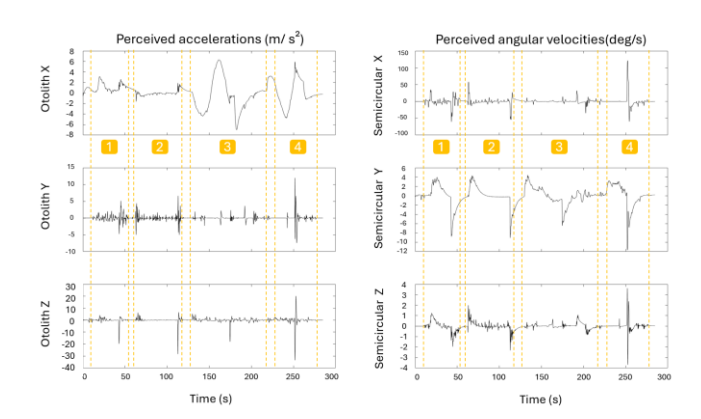


Figure 8: Perceived motion - Aggressive

Based on the spectral content analysis discussed in Section 2.2, the novel washout parameter set was defined by adjusting the filters' cutoff frequencies, as described in Section 2.4, and evaluating the resulting perceived error. For the translational channel, the updated natural frequencies (ω_n) were set to 0.782 rad/s for X, and 1.723 rad/s for both Y and Z. In the rotational channel the values for ω_n were updated to 1.42 rad/s for X, 0.75 rad/s for Y, and 0.8 rad/s for Z. Tilt coordination was tuned to $\omega_n = 1.564$ rad/s for X and 3.446 rad/s for Y. Lastly, for the rail channel, the cutoff frequency was set to 0.11 rad/s as defined in [1], and an additional change was made were the allowed travel range was expanded from ± 2 m to ± 3.5 m to permit wider range motion.

Figure 9 presents the Bode plots for both the baseline and tuned configurations. In the plots, "T" and "R" refer to the translational and rotational channels respectively, while "Tilt" and "Rail" denote the tilt coordination and rail channel components.

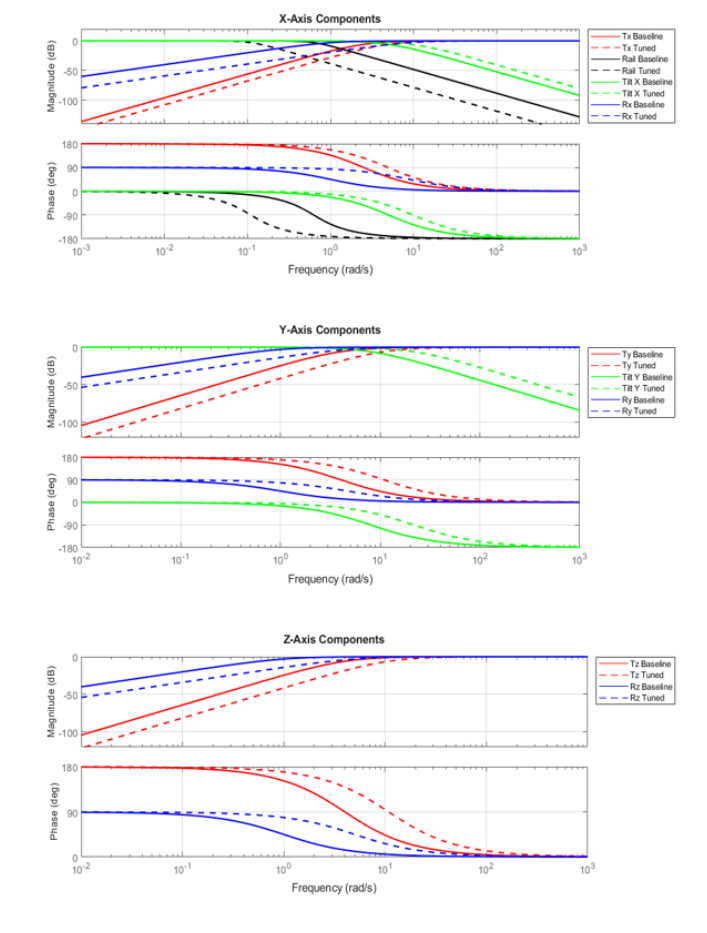


Figure 9: Bode plots of each channel for both MCAs

The error between the perceived motion shown in Figures 7 and 8 and the corresponding sensations delivered by the simulator is plotted in Figure 10 for the smooth run, and in Figure 11 for the aggressive one. These values were computed using the human perception thresholds applied, which contributes for the zero-mismatch regions observed in some signal segments.

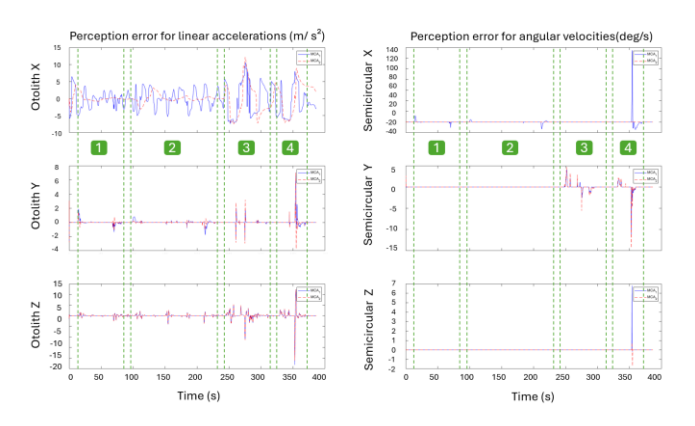


Figure 10: Perception error - Smooth

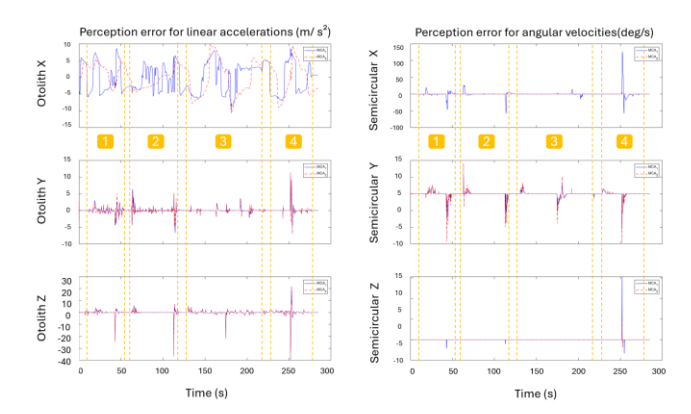


Figure 11: Perception error - Aggressive

Across both flight profiles, only the Otolith X, Semicircular X, and Semicircular Z channels exhibited notable differences between the baseline and tuned configurations. In all three cases, the tuned motion cueing delivered improved performance, with the enhancement being particularly evident in the Otolith X comparison.

It is worth noting the spike that appears at the beginning of some signals. This transient response results from the sudden repositioning of the SIVOR platform—from the robot's initial default posture to the position commanded by the motion cueing algorithm to align with the aircraft's initial dynamic state.

Another key factor considered during the filter tuning process is the potential for collisions between the simulator cockpit and the robotic arm. For this intent, only the rail range was modified, allowing extended travel, while the other degrees of freedom were kept constrained to preserve safety. Although SIVOR includes collision avoidance mechanisms to prevent accidents, these systems function by halting motion, which directly impairs motion fidelity. To ensure the validity of the perceived motion analysis, the recorded simulations of both flights, under both motion cueing algorithms, were reviewed in CoppeliaSim to visually inspect for collisions. This verification step is crucial to be checked, since if the model predicts zero perceived mismatch (suggesting a good cueing performance) but the simulation reveals a collision, the perceived motion from the model is invalid, as the actual simulator would not be capable of reproducing that motion.

In the event of a collision, CoppeliaSim highlights the SIVOR cockpit, as shown in Figure 12.

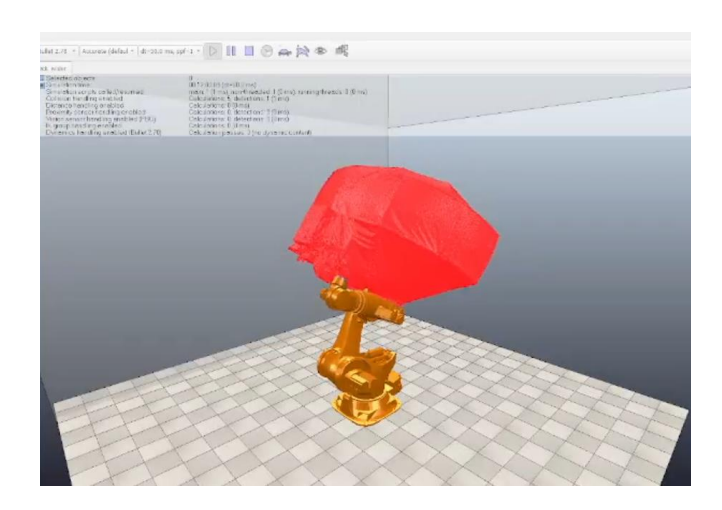


Figure 12: CoppeliaSim collision visualization from [19]

For the maneuvers performed in this experiment, no collisions were observed under either the baseline or the tuned washout configurations. While this is a positive outcome, for it avoids abrupt halts in platform motion, it does not necessarily indicate that the motion cueing is effective. An overly conservative washout filter can also result in collision-free operation by severely underutilizing the simulator's workspace, which is a special concern in highgain scenarios.

To assess performance quantitatively, Figure 13 presents the RMSE and cross-correlation (R) values for both motion cueing algorithms, with 'MCA 1' referring to the baseline and 'MCA 2' to the tuned configuration. The metrics are shown for the full flights (smooth and aggressive), as well as broken down by individual maneuver: M1 (180° turn), M2 (360° turn), M3 (loop), and M4 (Immelmann). Values below the human perception threshold are highlighted in bold.

Condition: Smooth		Whole Flight		M1		M2		M3		M4	
Pilot Vestibular - Output	Metric	MCA1	MCA2	MCA1	MCA2	MCA1	MCA2	MCA1	MCA2	MCA1	MCA2
Otolith - Ax	RMS	3,576	3,179	1,929	0,674	2,665	1,158	5,259	5,402	4,783	5,109
	Rxy	0,819	0,976	0,752	0,830	0,094	0,471	0,863	0,979	0,884	0,989
Otolith - Ay	RMS	0,407	0,357	0,217	0,140	0,249	0,133	0,324	0,371	0,930	0,854
	Rxy	0,039	-0,147	0,288	0,173	-0,014	-0,160	0,508	0,162	-0,038	-0,293
Otolith - Az	RMS	1,286	1,299	0,446	0,456	0,554	0,567	1,619	1,634	2,916	2,938
	Rxy	-0,076	-0,267	-0,025	-0,201	-0,056	-0,323	-0,048	-0,203	-0,094	0,330
Semicircular - Ox	RMS	6,251	6,662	2,138	2,542	2,331	2,822	0,651	0,924	17,110	17,910
	Rxy	0,426	0,238	0,362	0,212	0,543	0,187	0,715	0,198	0,396	0,241
Semicircular - Oy	RMS	1,475	1,527	0,614	0,653	0,497	0,541	2,413	2,389	2,747	2,955
	Rxy	0,238	0,213	0,041	-0,038	0,110	0,036	0,285	0,295	0,260	0,179
Semicircular - Oz	RMS	0,361	0,292	0,312	0,321	0,256	0,259	0,141	0,123	0,827	0,554
	Rxy	-0,016	0,012	0,122	-0,043	0,068	0,015	0,248	0,489	-0,223	0,005

Condition: Aggressive		Whole Flight		M1		M2		M3		M4	
Pilot Vestibular - Output	Metric	MCA1	MCA2	MCA1	MCA2	MCA1	MCA2	MCA1	MCA2	MCA1	MCA2
Otolith - Ax	RMS	4,437	4,488	4,768	3,404	3,500	2,810	4,614	5,643	4,939	5,215
	Rxy	0,850	0,970	0,904	0,949	0,051	0,461	0,933	0,990	0,811	0,968
Otolith - Ay	RMS	0,908	0,880	1,064	1,039	1,151	0,973	0,493	0,486	1,317	1,398
	Rxy	0,161	0,027	0,202	0,088	0,268	0,204	0,319	0,243	-0,004	-0,241
Otolith - Az	RMS	2,214	2,262	2,172	2,215	2,150	2,210	1,487	1,518	3,789	3,865
	Rxy	0,022	-0,167	0,095	-0,154	0,055	-0,155	-0,076	-0,185	0,016	-0,181
Semicircular - Ox	RMS	9,020	10,398	8,903	11,486	8,271	10,732	3,067	4,327	17,351	18,341
	Rxy	0,553	0,251	0,672	0,293	0,659	0,206	0,763	0,344	0,412	0,241
Semicircular - Oy	RMS	2,217	2,433	2,944	3,219	2,107	2,412	2,062	2,231	2,399	2,624
	Rxy	0,101	0,058	-0,026	-0,085	0,057	0,003	0,116	0,099	0,267	0,202
Semicircular - Oz	RMS	0,755	0,460	0,796	0,531	0,534	0,392	0,444	0,287	1,427	0,798
	Rxy	-0,055	0,029	0,191	0,137	0,030	0,126	-0,128	-0,015	-0,462	-0,067

Figure 13: RMSE and cross-correlation breakdown

From the results, we observe that for some channels, MCA 2 provides lower overall error during the full flight, but may yield higher error during specific maneuvers, and vice versa. Additionally, there are instances where a higher correlation coincides with greater error—or lower error with worse correlation—highlighting the importance of using both metrics in parallel when evaluating cueing fidelity. These findings also point out the limitation of the classical washout configuration, where the constant parametrization yields better performance in some cases while lacking in others.

4 Conclusion

The results of this analysis indicate that the classical washout filter configuration, although widely used in the simulation of commercial and transport aircraft, does not perform adequately in the context studied. Both the baseline and tuned versions of the filter failed to consistently deliver representative motion cues across the tested scenarios, highlighting the limitations of a fixed-parameter design.

While the tuned configuration showed modest improvements over the baseline in some aspects, it still exhibited significant shortcomings. Another important point demonstrated in the study is that performance varied not only between different maneuvers, but also within the same maneuver when different input profiles were used. This suggests that, regardless of careful offline tuning (e.g., in the case of optimization being applied) fixed-parameter washout filters cannot adequately adapt to the dynamic and varied demands of fighter aircraft motion. The inability to provide optimal cueing across all conditions emphasizes the need for more flexible strategies.

Ultimately, this work serves as motivation for future research into adaptive or model-predictive motion cueing algorithms. These approaches are more likely to handle both maneuver type and pilot input dynamics in real time, potentially enabling better use of SIVOR's workspace and more accurate representation of fighter jet motion across a wide range of scenarios.

5 Acknowledgments

This work was made possible through the financial support of FINEP by means of the Project ADS ("Cenários Futuros de Domínio Aéreo"), process no. 01.20.0195.00 and Project MMAS, process no. 01.22.0478.01 (1538/22).

References

- [1] Matheus, A. da C.; Oliveira, W. R. and Villani, E. "A Safety-Oriented Motion Cueing Algorithm for a Serial Robotic Flight Simulator Using a Predictive Neural Network Reference Governor," in *IEEE Transactions on Intelligent Transportation Systems*, vol. 25, no. 11, pp. 15718-15731, Nov. 2024, doi: 10.1109/TITS.2024.3442973.
- [2] R. Casas, et al., "On the objective evaluation of motion cueing in vehicle simulations," *Vehicle System Dynamics*, vol. 58, no. 2, pp. 1–15, 2020.
- [3] T. Naatal, A. Matheus, E. Villani, and W. R. de Oliveira, "Implementation analysis of a washout filter on a robotic flight simulator a case study," *Journal of Aerospace Systems*, vol. 5, no. 2, pp. 77–85, 2019.
- [4] M. Katliar, F. M. Drop, H. Teufel, M. Diehl, and H. H. Bülthoff, "Real-time nonlinear model predictive control of a motion simulator based on an 8-DOF serial robot," in *Proc. 2018 European Control Conference (ECC)*, Limassol, Cyprus, June 12–15, 2018.
- [5] S. F. Schmidt and B. Conrad, "Motion drive signals for piloted flight simulators," NASA Report CR-1601, 1970.

- [6] E. T. da Silva, S. D. Penna, M. A. D. Alves, W. R. Oliveira, E. Villani, and L. G. Trabasso, "Flight simulator assisted by a robotic motion platform SIVOR design and applications," in AIAA SciTech 2019 Forum, San Diego, CA, 2019.
- [7] L. Forssell and U. Nilsson, ADMIRE: The Aero-Data Model In a Research Environment, Version 4.0 – Model Description, FOI-R--1624--SE, Swedish Defence Research Agency (FOI), Dec. 2005.
- [8] D. Cleij, J. Venrooij, P. Pretto, D. M. Pool, M. Mulder, and H. H. Bülthoff, "Comparison between filter- and optimization-based motion cueing algorithms for driving simulation," *IEEE Transactions on Human-Machine Systems*, 2017.
- [9] D. Cleij, J. Venrooij, P. Pretto, D. M. Pool, M. Mulder, and H. H. Bülthoff, "Continuous rating of perceived visual-inertial motion incoherence during driving simulation," in *Proc. Driving Simulation Conference* (DSC) Europe, Tübingen, Germany, 2015, pp. 191–198.
- [10] L. Pollini and M. Innocenti, "Study of a novel motion platform for flight simulators using an anthropomorphic robot," in AIAA Modeling and Simulation Technologies Conference and Exhibit, Keystone, CO, USA, Aug. 21– 24, 2006.
- [11] W. R. de Oliveira, et al., "External dynamic behavior of an industrial robotic system," *IEEE/ASME Transactions on Mechatronics*, vol. 24, no. 3, pp. 1–8, 2019.
- [12] M. M. Momani and F. M. Cardullo, "A review of the recent literature on the mathematical modeling of the vestibular system," *Biomedical Engineering Letters*, vol. 8, pp. 223–236, 2018.
- [13] R. J. Telban and F. M. Cardullo, *Motion Cueing Algorithm Development: Human-Centered Linear and Nonlinear Approaches*, NASA/CR-2005-213747, 2005.
- [14] M. Vargas, Controle de uma plataforma de movimento de um simulador de voo (in Portuguese), PhD thesis, Universidade de São Paulo, São Paulo, Brazil, 2009.
- [15] Wesley R. de Oliveira, A. Matheus., G. Rodamilans, R. Nicola, D. Arjoni, L. G. Trabasso, E. Villani. Evaluation of the Pilot Perception in a Robotic Flight Simulator with and without a Linear Unit. In: AIAA Scitech 2019 Forum, 2019, San Diego. AIAA Scitech 2019 Forum. Reston: AIAA, 2019. DOI: 10.2514/6.2019-0713.
- [16] A. Nesti, C. Masone, M. Barnett-Cowan, P. R. Giordano, H. H. Bülthoff, and P. Pretto, "Roll rate thresholds and perceived realism in driving simulation,"

- in *Proc. Driving Simulation Conference (DSC)*, 2012, pp. 23–31.
- [17] MathWorks, "rmse," MATLAB Documentation.
 [Online]. Available:
 https://www.mathworks.com/help/matlab/ref/rmse.htm
 <a href
- [18] Buck, John R., Michael M. Daniel, and Andrew C. Singer. Computer Explorations in Signals and Systems Using MATLAB®. 2nd Edition. Upper Saddle River, NJ: Prentice Hall, 2002.
- [19] C. C. D. da Silva, Y. Castro, A. Sarmento, and E. Villani, "Multiplatform simulation using ROS," in Proc. 34th Congress of the International Council of the Aeronautical Sciences (ICAS), Florence, Italy, 2024.